1

Natural Motions of Rigid Spacecraft

1.1 Translational Motions in Space

The natural motions of the center of mass of a body in space are described by Newton's equations:

$$m \overset{I}{\vec{v}} = \vec{F}, \tag{1.1}$$

$$\overset{I}{\vec{r}} = \vec{v}, \tag{1.2}$$

where

m = mass of the spacecraft,

$(\vec{v}, \vec{r})$ = (velocity, position) of the center of mass with respect to inertial space,

$\overset{I}{(\ )}$ = time rate of change with respect to inertial space,

$\vec{F}$ = sum of external forces.

In the absence of external forces, the velocity stays constant, and the position changes linearly with time.

For motions taking place in times very much less than an orbit period (either around the Sun or the Earth), neglecting gravity yields a useful approximation for the translational motions.

1.2 Translational Motions in Circular Orbit

In circular orbit, centrifugal force balances gravitational force. For *small deviations from circular orbit*, the equations of motion of the center of mass are conveniently written in locally-horizontal-vertical (LHV) coordinates that rotate with the orbital angular velocity, n (see Fig. 1.1):

$$\delta \overset{I}{\vec{v}} \equiv \delta \overset{L}{\vec{v}} + \vec{\omega}_L \times \delta\vec{v} = \delta\vec{F}/m, \tag{1.3}$$

$$\delta \overset{I}{\vec{r}} = \delta \overset{L}{\vec{r}} + \vec{\omega}_L \times \delta\vec{r} = \delta\vec{v}, \tag{1.4}$$

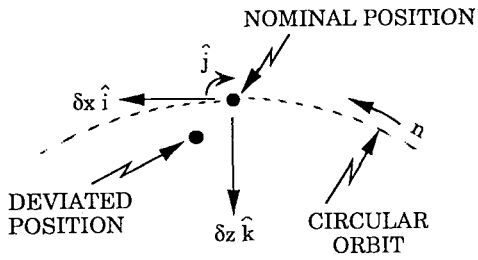

Figure 1.1. Locally-horizontal-vertical (LHV) coordinates for position deviation from circular orbit.

where

$\delta\vec{v}$ = velocity deviation,

$\delta\vec{r}$ = position deviation,

$\delta\vec{F}$ = force deviation,

$\overset{L}{(\ )}$ = denotes time derivative of components with respect to LHV axes,

$\vec{\omega}_L$ = angular velocity of LHV axes with respect to inertial axes.

Following NASA standard notation, δx is in-track position deviation (positive in direction of orbital velocity), δy is cross-track position deviation, and δz is vertical deviation (positive down). Thus,

$$\delta\vec{v} = \hat{\imath}\delta u + \hat{\jmath}\delta v + \hat{k}\delta w, \tag{1.5}$$

$$\delta\vec{r} = \hat{\imath}\delta x + \hat{\jmath}\delta y + \hat{k}\delta z, \tag{1.6}$$

$$\vec{\omega}_L = -n\hat{\jmath}, \tag{1.7}$$

where $n \triangleq \sqrt{g/R}$ = orbital angular velocity and $(\hat{\imath},\ \hat{\jmath},\ \hat{k})$ are unit vectors along the $(x,\ y,\ z)$ axes. The only force is the inverse-square gravitational force

$$\vec{F} = mg\left(\frac{R}{R-\delta z}\right)^2 \hat{k}, \tag{1.8}$$

where g = gravitational force per unit mass at radial distance, R, from the attracting center. Thus the deviation in force is given by

$$\delta\vec{F} = 2mg\frac{R^2\delta z}{(R-\delta z)^3}\hat{k} + mg\left(\frac{R}{R-\delta z}\right)^2\left(\frac{\partial\hat{k}}{\partial x}\delta x + \frac{\partial\hat{k}}{\partial y}\delta y\right), \tag{1.9}$$

and

$$\frac{\partial \hat{k}}{\partial x} = -\frac{1}{R}\hat{\imath}, \tag{1.10}$$

$$\frac{\partial \hat{k}}{\partial y} = -\frac{1}{R}\hat{\jmath}. \tag{1.11}$$

Substituting (5)–(7) and (9)–(11) into (1) and (2), we obtain the equations of motion for small deviations from circular orbit. They decouple into a set governing *cross-track motions*

$$\begin{bmatrix} \delta\dot{v} \\ \delta\dot{y} \end{bmatrix} = \begin{bmatrix} 0 & -n^2 \\ 1 & 0 \end{bmatrix} + \begin{bmatrix} T_y/m \\ 0 \end{bmatrix} \tag{1.12}$$

and a set governing *in-track/radial motions*

$$\begin{bmatrix} \delta\dot{u} \\ \delta\dot{w} \\ \delta\dot{x} \\ \delta\dot{z} \end{bmatrix} = \begin{bmatrix} 0 & n & -n^2 & 0 \\ -n & 0 & 0 & 2n^2 \\ 1 & 0 & 0 & n \\ 0 & 1 & -n & 0 \end{bmatrix} \begin{bmatrix} \delta u \\ \delta w \\ \delta x \\ \delta z \end{bmatrix} + \begin{bmatrix} T_x/m \\ T_z/m \\ 0 \\ 0 \end{bmatrix} \tag{1.13}$$

where (T_x, T_y, T_z) = thrust components.

The characteristic equation of the system (12) is

$$s^2 + n^2 = 0, \tag{1.14}$$

so there is one purely oscillatory mode at frequency n. The natural motion is of the form

$$\begin{bmatrix} \delta v \\ \delta y \end{bmatrix} = c \begin{bmatrix} n \\ 0 \end{bmatrix} \cos(nt + \beta) - c \begin{bmatrix} 0 \\ -1 \end{bmatrix} \sin(nt + \beta), \tag{1.15}$$

where c and β are arbitrary constants, and the complex eigenvector corresponding to $s = nj$ is $(n, -j)^T$. The real part of this eigenvector is the coefficient of

$\cos(nt + \beta)$, while the imaginary part is the coefficient of $[-\sin(nt + \beta)]$. The motion may be interpreted as a slight change in orbit plane, so that the spacecraft crosses the reference orbital plane twice per revolution, and thus appears to oscillate right-left with orbital frequency n.

The characteristic equation of the system (13) is

$$s^2(s^2 + n^2) = 0, \tag{1.16}$$

so there is one purely oscillatory mode at frequency n, and two stationary modes. The natural motions are of the form

$$\begin{bmatrix} \delta u \\ \delta w \\ \delta x \\ \delta z \end{bmatrix} = c_1 \begin{bmatrix} 0 \\ n \\ 2 \\ 0 \end{bmatrix} \cos(nt + \beta) - c_1 \begin{bmatrix} n \\ 0 \\ 0 \\ 1 \end{bmatrix} \sin(nt + \beta) + (c_2 + c_3 nt) \begin{bmatrix} 0 \\ n \\ 1 \\ 0 \end{bmatrix} + c_3 \begin{bmatrix} n/3 \\ 0 \\ 0 \\ 2/3 \end{bmatrix}, \tag{1.17}$$

where c_1, β, c_2, and c_3 are arbitrary constants. The first two column vectors in (17) are the real and imaginary parts of the eigenvector corresponding to $s = nj$; the third and fourth column vectors are the principal and secondary eigenvectors corresponding to $s = 0$ (see Appendix A). The motion of the perturbed spacecraft in each of these three modes, as observed from an unperturbed spacecraft in the same circular orbit, is shown in Fig. 1.2.

The first mode ($c_1 \neq 0$) corresponds to a slightly elliptic orbit so that the spacecraft goes above the circular orbit for half a period and slows down, then goes below and speeds up for the other half. The second mode ($c_2 \neq 0$) corresponds to the spacecraft being in the same circular orbit but slightly ahead of (or behind) the reference point. The third mode ($c_3 \neq 0$) corresponds to the spacecraft being in a lower (or higher) circular orbit that has a faster (or slower) orbital velocity.

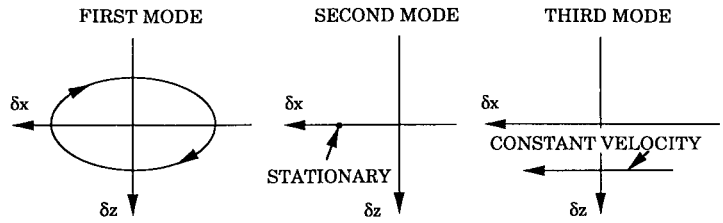

Figure 1.2. Modes of translational motion in circular orbit.

1.3 Rotational Motions in Space

The rotational (attitude) motions of a rigid spacecraft in space are described by Euler's equations:

$$\overset{I}{\vec{H}} \equiv \overset{B}{\vec{H}} + \vec{\omega} \times \vec{H} = \vec{Q}, \tag{1.18}$$

where

$\vec{H}$ = $\vec{\vec{I}} \cdot \vec{\omega}$ = moment of momentum of spacecraft about the c.m.,

$\vec{\vec{I}}$ = moment of inertia dyadic with respect to the c.m. of the S/C,

$\vec{\omega}$ = angular velocity of S/C with respect to inertial space,

$\overset{B}{(\ )}$ = time rate of change with respect to body-fixed axes,

$\vec{Q}$ = resultant external torque.

Since the moment of inertia dyadic, $\vec{\vec{I}}$, is constant in body-fixed axes, Equation (18) is usually used in body-axis components. If the body-axis components of the angular velocity are $(p, q, r) \Rightarrow \vec{\omega} = p\hat{\imath} + q\hat{\jmath} + r\hat{k}$ and we use principal axes so that $\vec{\vec{I}} = I_x\hat{\imath}\hat{\imath} + I_y\hat{\jmath}\hat{\jmath} + I_z\hat{k}\hat{k}$, where ($\hat{\imath}$, $\hat{\jmath}$, $\hat{k}$ are unit vectors along the (x, y, z) principal body axes, then (1) becomes

$$I_x\dot{p} - (I_y - I_z)qr = Q_x, \tag{1.19}$$

$$I_y\dot{q} - (I_z - I_x)rp = Q_y, \tag{1.20}$$

$$I_z\dot{r} - (I_x - I_y)pq = Q_z, \tag{1.21}$$

where (Q_x, Q_y, Q_z) are the body-axis components of the torque.

1.3.1 *Kinematic Equations*

Angular position may be described by three *Euler angles* (or by four Euler parameters (quaternions), or nine direction cosines (cf. Kane)). The NASA

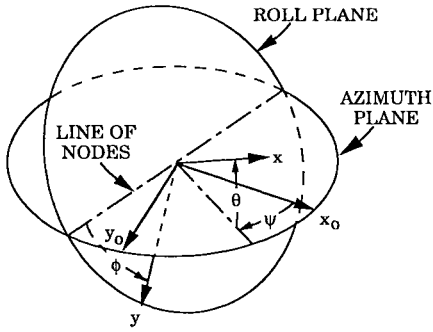

Figure 1.3. Aerospace euler angles (NASA standard).

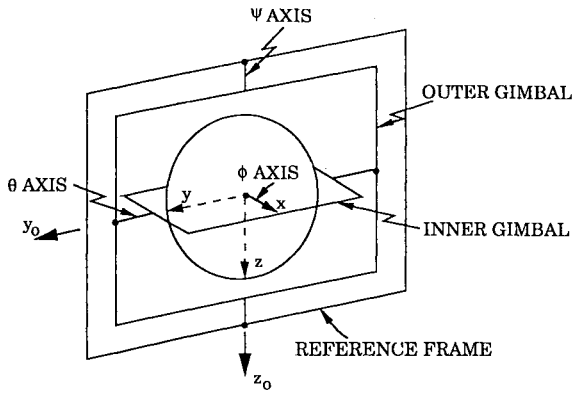

Figure 1.4. Two-gimbal interpretation of aerospace euler angles.

standard Euler angles are shown in Fig. 1.3; the first rotation, ψ, is about the body z-axis; the second rotation, θ, is about the new position of the body y-axis; the third rotation, ϕ, is about the new position of the body x-axis. Fig. 1.4 shows a two-gimbal interpretation of these Euler angles. If the body-axis components of the angular velocity are (p, q, r), then the Euler angle rates are

$$\begin{bmatrix} \dot{\phi} \\ \dot{\theta} \\ \dot{\psi} \end{bmatrix} = \frac{1}{\cos\theta} \begin{bmatrix} \cos\theta & \sin\theta\sin\phi & \sin\theta\cos\phi \\ 0 & \cos\theta\cos\phi & -\cos\theta\sin\phi \\ 0 & \sin\phi & \cos\phi \end{bmatrix} \begin{bmatrix} p \\ q \\ r \end{bmatrix}. \tag{1.22}$$

1.3.2 *Small Attitude Changes of a Nonspinning Spacecraft*

For small attitude changes of a nonspinning spacecraft with respect to inertial space, that is, magnitudes of ϕ, θ, ψ small compared to unity, the nonlinear equations of motion (19)–(22) are well approximated by the following *linearized equations of motion*:

$$I_x\dot{p} \cong Q_x, \tag{1.23}$$

$$I_y\dot{q} \cong Q_y, \tag{1.24}$$

$$I_z\dot{r} \cong Q_z, \tag{1.25}$$

$$\dot{\phi} \cong p, \tag{1.26}$$

$$\dot{\theta} \cong q, \tag{1.27}$$

$$\dot{\psi} \cong r. \tag{1.28}$$

Thus angular motion about each of the three principal axes is uncoupled from motion about the other two principal axes. Eliminating (p, q, r) from (23)–(28), we obtain three independent second-order systems:

$$I_x\ddot{\phi} \cong Q_x, \tag{1.29}$$

$$I_y\ddot{\theta} \cong Q_y, \tag{1.30}$$

$$I_z\ddot{\psi} \cong Q_z. \tag{1.31}$$

1.4 Rotational Motions in Circular Orbit

1.4.1 *Gravity Torque*

The very small torque acting on a rigid body in an inverse-square gravitational field may be written as

$$\vec{Q}_g = 3\frac{g}{R}\hat{r} \times (\vec{\vec{I}} \cdot \hat{r}), \tag{1.32}$$

where

g = gravitational force per unit mass at radial distance R,

$\hat{r}$ = unit vector in the radial direction,

$\vec{\vec{I}}$ = moment-of-inertia dyadic of the rigid body.

This torque is zero whenever a principal axis is parallel to $\hat{r}$, since $\vec{\vec{I}} \cdot \hat{r} = \lambda\hat{r}$ and $\hat{r} \times (\lambda\hat{r}) = 0$.

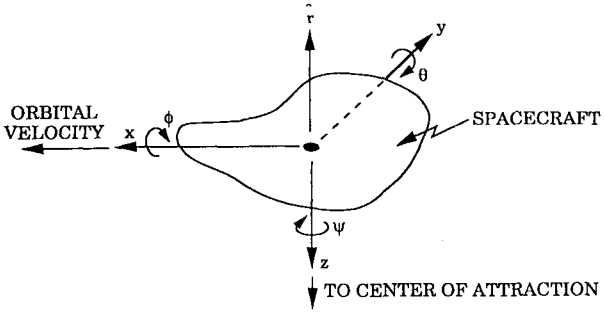

Figure 1.5. Nominal attitude and small-deviation angles for spacecraft in circular orbit.

If the body principal axes (x, y, z) are aligned as shown in Fig. 1.5, then

$$\vec{I} = I_x \hat{\imath}\hat{\imath} + I_y \hat{\jmath}\hat{\jmath} + I_z \hat{k}\hat{k}, \tag{1.33}$$

where (I_x, I_y, I_z) are the principal moments of inertia and $(\hat{\imath}, \hat{\jmath}, \hat{k})$ are unit vectors pointing along the body (x, y, z) axes.

For small angular departures from this nominal position

$$\begin{aligned} \hat{r} &\cong \theta\hat{\imath} - \phi\hat{\jmath} - \hat{k}, \\ \Rightarrow \vec{I}\cdot\hat{r} &\cong I_x\theta\hat{\imath} - I_y\phi\hat{\jmath} - I_z\hat{k}, \\ \Rightarrow \hat{r}\times(\vec{I}\cdot\hat{r}) &\cong (I_z - I_y)\phi\hat{\imath} + (I_z - I_x)\theta\hat{\jmath} + (I_x - I_y)\overbrace{\phi\theta\hat{k}}^{\text{Negligible}}. \end{aligned} \tag{1.34}$$

1.4.2 *Relationship between Euler Angle Rates and Angular Velocity*

Let (p, q, r) be body-axis components of the angular velocity of the body with respect to inertial axes, and let (ϕ, θ, ψ) be Euler angles of the body axes with respect to locally horizontal axes, (LHA). Then

$$\begin{bmatrix} p \\ q \\ r \end{bmatrix} = \begin{bmatrix} \dot{\phi} \\ 0 \\ 0 \end{bmatrix} + T_\phi \begin{bmatrix} 0 \\ \dot{\theta} \\ 0 \end{bmatrix} + T_\phi T_\theta \begin{bmatrix} 0 \\ 0 \\ \dot{\psi} \end{bmatrix} + T_\phi T_\theta T_\psi \begin{bmatrix} 0 \\ -n \\ 0 \end{bmatrix}, \tag{1.35}$$

where n = angular velocity of LHA with respect to inertial axes and

$$T_\phi = \begin{bmatrix} 1 & 0 & 0 \\ 0 & c\phi & s\phi \\ 0 & -s\phi & c\phi \end{bmatrix}, \; T_\theta = \begin{bmatrix} c\theta & 0 & -s\theta \\ 0 & 1 & 0 \\ s\theta & 0 & c\theta \end{bmatrix}, \; T_\psi = \begin{bmatrix} c\psi & s\psi & 0 \\ -s\psi & c\psi & 0 \\ 0 & 0 & 1 \end{bmatrix}. \tag{1.36}$$

A useful mnemonic for these rotations (thanks to Professor Holt Ashley) is $-s(\ )$ is above the row with a 1 in it, cyclically.

From (35) and (36) it follows that

$$\begin{bmatrix} p \\ q \\ r \end{bmatrix} = \begin{bmatrix} 1 & 0 & -s\theta \\ 0 & c\phi & c\theta s\phi \\ 0 & -s\phi & c\theta c\phi \end{bmatrix} \begin{bmatrix} \dot{\phi} \\ \dot{\theta} \\ \dot{\psi} \end{bmatrix} - \begin{bmatrix} s\psi c\theta \\ s\psi s\theta s\phi + c\psi c\phi \\ s\psi s\theta c\phi - c\psi s\phi \end{bmatrix} n. \tag{1.37}$$

If (ψ, θ, ϕ) are small in magnitude compared to 1 radian, then (37) may be approximated by

$$\begin{aligned} p &\cong \dot{\phi} - n\psi - \dot{\psi}\theta, \\ q &\cong \dot{\theta} - n + \dot{\psi}\phi, \\ r &\cong \dot{\psi} + n\phi - \dot{\theta}\phi. \end{aligned} \tag{1.38}$$

The average value, over an orbit period, of the magnitude of the nonlinear terms $(\dot{\psi}\theta, \dot{\psi}\phi, \dot{\theta}\phi)$ in (38) is small compared to the average magnitude of the linear terms if ϕ and θ are oscillatory about zero or if the magnitudes of $\dot{\psi}$ and $\dot{\theta}$ are small compared to the orbit rate n. In such cases, (38) may be approximated as

$$\begin{aligned} \dot{\phi} &\cong p + n\psi, \\ \dot{\theta} &\cong q + n, \\ \dot{\psi} &\cong r - n\phi. \end{aligned} \tag{1.39}$$

1.4.3 *Moment of Momentum*

The angular velocities of a rigid spacecraft may be determined from Euler's equations for moment of momentum:

$$\overset{I}{\vec{H}} \equiv \overset{B}{\vec{H}} + \vec{\omega}^{B-I} \times \vec{H} = \vec{Q}, \tag{1.40}$$

where

$\vec{H}$ = $\vec{\vec{I}} \cdot \vec{\omega}$ = moment of momentum,

$\vec{\omega}$ = $\vec{\omega}^{B-I}$ = angular velocity body with respect to inertial space,

$\vec{Q}$ = external torques on body.

1.4.4 *Equations of Motion, Earth-Pointing Satellite*

Assuming that the body axes are principal axes, the moment of momentum of the spacecraft is

$$\vec{H} = I_x p\hat{\imath} + I_y q\hat{\jmath} + I_z r\hat{k}. \tag{1.41}$$

From (32), (34), (39), and (40), the equations of motion for small perturbations from locally horizontal axes decouple into two sets, one for pitch and one for roll/yaw. The pitch set is:

$$I_y\dot{q} \cong -3n^2(I_x - I_z)\theta + Q_y, \tag{1.42}$$

$$\dot{\theta} - n \cong q. \tag{1.43}$$

The roll/yaw set is

$$I_x\dot{p} + n(I_y - I_z)r \cong -3n^2(I_y - I_z)\phi + Q_x, \tag{1.44}$$

$$I_z\dot{r} - n(I_y - I_x)p \cong Q_z, \tag{1.45}$$

$$\dot{\phi} - n\psi \cong p, \tag{1.46}$$

$$\dot{\psi} + n\phi \cong r, \tag{1.47}$$

where $n \triangleq \sqrt{g/R}$ = orbital angular velocity and (Q_x, Q_y, Q_z) are external torques. The gyroscopic coupling terms, $n(I_y - I_z)r$ in (44) and $n(I_y - I_x)p$ in (45), arise from the rotation of the locally horizontal axes at orbit rate n.

1.4.5 *Pitch Librations*

The characteristic equation of the pitch system (Equations (42) and (43)) in circular orbit is

$$s^2 + 3n^2\frac{I_x - I_z}{I_y} = 0. \tag{1.48}$$

If $I_x > I_z$, the system has undamped oscillations (librations) at a frequency

$$\omega_p = \sqrt{\frac{3(I_x - I_z)}{I_y}}n, \tag{1.49}$$

which is called the pitch libration frequency. If $I_x < I_z$, the system is unstable.

1.4.6 *Roll/Yaw Librations*

Eliminating p and r from Equations (44)–(47), the Laplace transform of the roll/yaw equations may be written as

$$\begin{bmatrix} s^2 + 4an^2 & (a-1)ns \\ -(b-1)ns & s^2 + bn^2 \end{bmatrix} \begin{bmatrix} \phi(s) \\ \psi(s) \end{bmatrix} = \begin{bmatrix} Q_x(s)/I_x \\ Q_z(s)/I_z \end{bmatrix}. \tag{1.50}$$

where

$$a \triangleq (I_y - I_z)/I_x, \tag{1.51}$$

$$b \triangleq (I_y - I_x)/I_z. \tag{1.52}$$

The characteristic equation of (50) is

$$\left(\frac{s}{n}\right)^4 + (3a + ab + 1)\left(\frac{s}{n}\right)^2 + 4ab = 0. \tag{1.53}$$

The magnitudes of a and b are less than or equal to unity since

$$\begin{aligned} a &= \frac{\int\int\int(x^2+z^2)dm - \int\int\int(x^2+y^2)dm}{\int\int\int(y^2+z^2)dm}, \\ &= \frac{\int\int\int(z^2-y^2)dm}{\int\int\int(z^2+y^2)dm}, \end{aligned}$$

and similarly

$$b = \frac{\int\int\int(x^2-y^2)dm}{\int\int\int(x^2+y^2)dm}.$$

For b = constant, (53) may be written in Evan's root locus form as

$$-a(3+b) = \frac{s^2(s^2+1)}{s^2 + 4b/(3+b)}, \tag{1.54}$$

where s is in units of n. Fig. 1.6 shows the root loci vs. a for fixed values of b, and Fig. 1.7 summarizes the results. The spacecraft roll/yaw motions are oscillatory for $a > 0$, $b > 0$, and for a small region when $a < 0$, $b < 0$; elsewhere the motions are unstable.

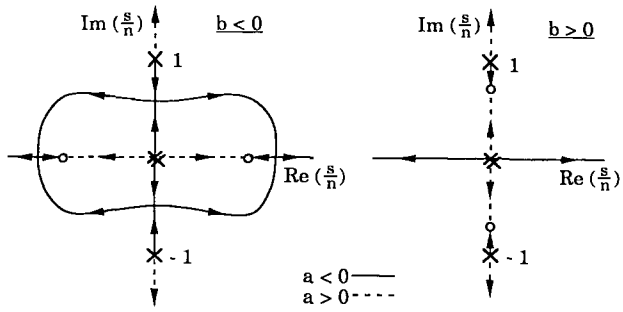

Figure 1.6. Root loci vs. moment-of-inertia ratio $a = (I_y - I_z)/I_x$) for roll/yaw motions.

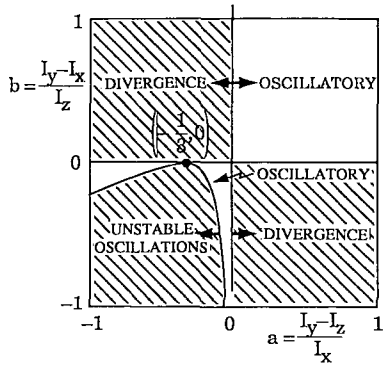

Figure 1.7. Unstable regions for roll/yaw motions of spacecraft in circular orbit.

1.4.7 *Roll/Yaw Librations of Axially Symmetric Spacecraft*

Symmetry Axis Nominally Vertical

Here $I_x = I_y$, which implies $b = 0$, and $a = 1 - I_z/I_x$. For $0 < a < 1$, the spacecraft is prolate whereas for $-1 < a < 0$ the spacecraft is oblate. The characteristic equation for this case ((53) with $b = 0$)) is

$$s^2[s^2 + (3a + 1)n^2] = 0. \tag{1.55}$$

The double pole at $s = 0$ represents the yaw mode, which is uncoupled to roll motions. The roll mode is oscillatory if $a > -1/3$ or $I_z/I_x < 4/3$ (prolate spacecraft); it is unstable if $I_z/I_x > 4/3$ (oblate spacecraft).

Symmetry Axis Nominally In-Track

Here $I_y = I_z$, which implies $a = 0$, and $b = 1 - I_x/I_z$. The characteristic equation for this case is

$$s^2(s^2 + n^2) = 0. \tag{1.56}$$

One of the $s = 0$ poles represents a roll-angle-indifference mode, that is, $\phi =$ constant $\neq 0$, $\psi = 0$. The other $s = 0$ pole represents a mode with constant roll rate, $\dot{\phi}$, and a constant yaw angle ψ, where

$$\psi = \frac{b-1}{b}\frac{\dot{\phi}}{n}, \tag{1.57}$$

that is, a stationary attitude of the symmetry axis with respect to the locally horizontal axes. The other mode is oscillatory with frequency = n, that is, a stationary attitude of the symmetry axis with respect to inertial axes.

Axis of Symmetry Nominally Cross-Track

Here $I_x = I_z$, which implies $a = b = I_y/I_x - 1$. The characteristic equation for this case is

$$s^4 + (3a + a^2 + 1)n^2s^2 + 4a^2n^4 = 0. \tag{1.58}$$

The motions are oscillatory if $a > -.146$, or $I_y/I_x > .854$ (spacecraft oblate).

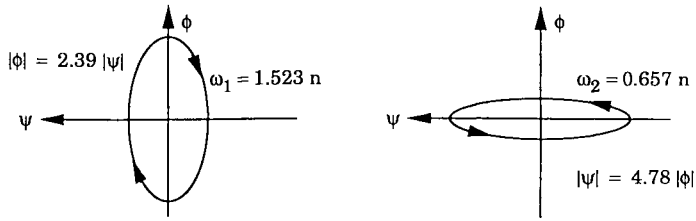

Figure 1.8. Path of tip of symmetry axis for librating oblate spacecraft with symmetry axis nominally cross-track.

Problem 1.4.1 – *Roll/Yaw Libration Modes for an Oblate Axially Symmetric Spacecraft*

Consider the roll/yaw libration motions of an oblate axially symmetric spacecraft with its symmetry axis nominally cross-track, where $I_x = I_z = 2/3I_y \Rightarrow a = b = 1/2$.

Show that the natural motions as viewed by an observer who is stationary with respect to the locally horizontal-vertical axes in circular orbit consist of a superposition

of two purely oscillatory modes with frequencies $\omega_1 = 1.523n$, $\omega_2 = .657n$, where the tip of the symmetry axis moves in elliptical paths as shown in Fig. 1.8. Note tip rotates in opposite directions for the two modes.

1.5 Disturbances

In the solar system, away from any planets, a spacecraft is in orbit about the sun. The main disturbance is solar radiation pressure, which is 4.4×10^{-6} Newtons per square meter at the earth's distance from the sun. By careful design, the solar radiation torque can be reduced to 10^{-5} or even 10^{-6} Newton-meters at the earth's distance from the sun.

Another significant disturbance is gas leakage from reaction control systems. Again, by careful design, this torque can be held to values on the order of 10^{-5} Newton-meters.

Moving mechanical parts and crew movements cause internal torques that disturb the attitude of the spacecraft and may cause significant flexural vibrations.

Fig. 1.9 (Ref. DE) shows typical disturbance torques on a spacecraft as a function of altitude above the earth's surface. Gravity torque is caused by the earth's gravity gradient (see Section 4.2). Magnetic torque is caused by the earth's magnetic field acting on the residual magnetic dipole moment of the spacecraft (see Section 4.4). Aerodynamic torque becomes significant below an altitude of 1000 kilometers.

All five of the disturbance torques in Fig. 1.9 can also be used as control torques. A controlled gas leak is a thruster; a solar sail uses radiation pressure; gravity, magnetic, and aerodynamic torques can be (and have been) used for desaturating reaction or momentum wheels (see Chapters 4 and 6).

During thrust maneuvers, the thrust misalignment torque is orders of magnitude larger than the torques mentioned here. Consequently, a special attitude control system is required during thrust maneuvers.

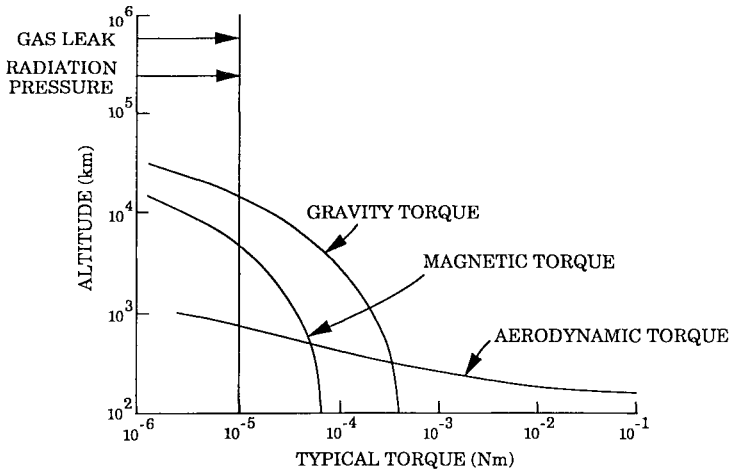

Figure 1.9. Typical torques on a small spacecraft as a function of orbital altitude.

2

Spacecraft Sensors and Attitude Determination

2.1 Introduction

In this chapter, we discuss a few of the many sensors that have been used for attitude determination, and some of the methods used to estimate attitude angles that are not directly sensed. A very thorough treatment is given in the book edited by Wertz (Ref. WE).

Most spacecraft in circular or elliptic orbits are stabilized with one body axis pointing downward so that cameras or antennas point toward the earth. Horizon sensors can then be used to measure the pitch and roll angles of the S/C. Adding roll-rate and yaw-rate gyros allows the yaw angle to be estimated using the knowledge of kinematic roll/yaw coupling (a process called "orbital gyro-compassing").

Many spacecraft have solar cells for generating electrical power from the sun's radiation, so some means must be provided for pointing solar panels toward the sun while the antennas/cameras point toward the earth; this requires a slow rotation of the panels with respect to the S/C, which changes the moments of inertia of the overall S/C.

Some spacecraft, particularly those whose missions involve scientific exploration, are stabilized so that the attitude is fixed with respect to inertial space. Thus, in circular orbit, the attitude with respect to the earth is constantly changing, like the cars on a ferris wheel.

Spinning S/C usually have the spin axis perpendicular to the orbit plane, except in transfer orbits. In order to have cameras or antennas pointing toward the earth and still have the advantage of spin stabilization, part of the S/C is de-spun (thus the term "dual-spin" S/C). Alternatively, a nonspinning S/C may contain a "bias momentum wheel" that provides spin stabilization.

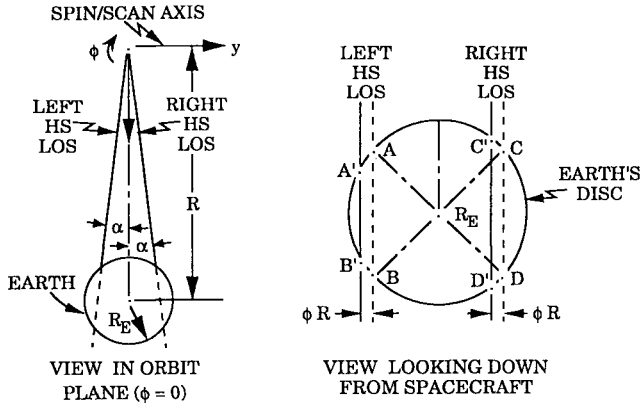

Figure 2.1. Geometry of spacecraft with two scanning horizon sensors.

2.2 Infra-Red, Optical, and Radar Sensors

2.2.1 *Horizon Sensors*

The earth's horizon is distinguished most sharply in infrared (IR) wavelengths, and IR sensors are less susceptible to sun interference than optical sensors.

A scanning mechanism is required because of the large angle subtended by the earth in circular orbit. For spinning S/C, the sensor is simply mounted on the S/C body. For nonspinning S/C, the sensor may either be mounted on a bias momentum wheel (which is also used for S/C attitude stabilization), or scanned with oscillating mirrors.

For spin-scan sensors, the times at which the sensor axis enters and leaves the earth's disc can be used to determine both pitch and roll angles. At the average of these two times, the sensor axis has zero pitch angle, so the angle between the z-axis of the de-spun part of the S/C and the sensor axis at that time is the S/C pitch angle θ. The difference between the two times is the time to cross the disc; knowing the altitude of the S/C, and the spin/scan speed, the magnitude (but not the sign) of the roll angle can be calculated.

More accurate sensing of the roll angle, ϕ, along with its sign, can be obtained with two spinning sensors whose axes diverge slightly (see Fig. 2.1). At zero roll angle the lines of sight (LOS) of the two sensors pass over the earth's disc with equal chords ($AB = CD$). When ϕ is not zero, one chord ($C'D'$ in Fig. 2.1) is longer than the other ($A'B'$). From measurements of the entry and exit times, ϕ can be determined quite accurately.

Problem 2.2.1 – *Analysis of Scanning Horizon Sensor*

Fig. 2.1 was simplified somewhat for clarity. The horizon sensor line of sight (LOS) actually moves on the surface of a cone, which intersects the (almost) spherical (earth + atmosphere). The entry and exit points (A', C' and B', D') occur when the LOS is just tangent to the sphere.

Express the pitch angle θ and the roll angle ϕ in terms of the entry and exit times t_A, t_C and t_B, t_D, the spin/scan angular velocity, the radius of the orbit R, and the sphere radius R_E.

2.2.2 *V-Beam Optical Slit Sensors*

A V-beam slit sensor consists of two photocells mounted in slits that form a V as shown in Fig. 2.2. The photocells are illuminated ("pulsed") by the sun (or the earth or the moon) once each rotation of a spinning spacecraft (or rotor section of a dual-spin spacecraft). The time difference between successive pulses of photocell S_1 (the "spin-angle sensor") is the rotation period, which determines the spin rate very precisely. The time difference between pulses of photocell S_1 and photocell S_2 (the "ϕ-angle sensor") is a function of the spin rate and the angle that the spin axis makes with the sun line, ϕ. Hence it can be used, with the spin rate, to determine ϕ.

The spin-angle sensor S_1 is pulsed when the sun's rays are perpendicular to the normal to the plane DS_1E. The ϕ-angle sensor S_2 is pulsed when the sun's rays are perpendicular to the normal to plane CS_2E.

Fig. 2.2 shows the case when the spin axis is perpendicular to the sun's rays ($\phi = 90$ deg), while Fig. 2.3 shows the case when the spin axis makes an angle

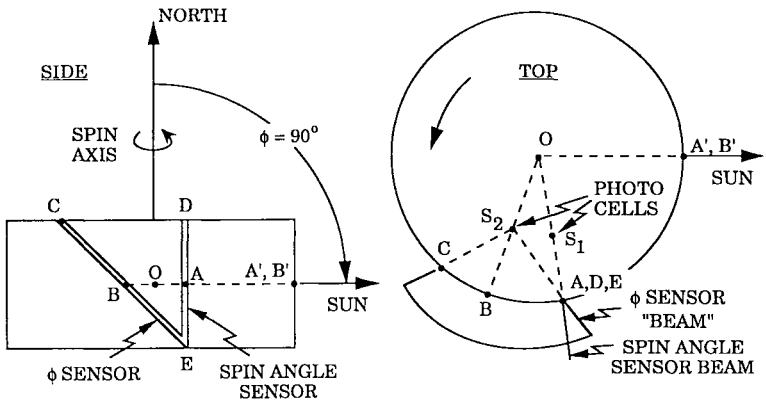

Figure 2.2. V-beam slit sensor on a spinning spacecraft—spin axis normal to the sun's rays.

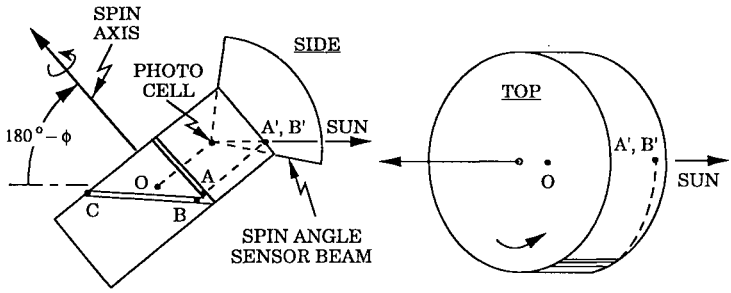

Figure 2.3. V-beam slit sensor on a spinning spacecraft—spin axis not normal to the sun's rays.

$>$ 90 deg with the sun line. The photocells are pulsed when the lines OA and OB are parallel to the sun line in postion OA' and OB'. The larger ϕ is, the shorter the time between the pulses.

Analysis of the V-Beam Slit Sensor

With reference to Fig. 2.4, let β = the azimuthal angle between the two photocells, $\vec{S}$ = sun line vector, $\vec{N}_1$ = normal to the spin angle sensor slit, $\vec{N}_2$ = normal to the ϕ angle sensor slit, $\alpha = \pi/2-$ angle between the spin axis and $\vec{N}_2$. The sun pulses sensor 1 when $\lambda = 0$ ($\vec{S} \cdot \vec{N}_1 = 0$); it pulses sensor 2 when ($\vec{S} \cdot \vec{N}_2 = 0$), that is, when

$$0 = \left(\hat{\imath}\sin\phi + \hat{k}\cos\phi\right) \cdot \left[\cos\alpha\cos\left(\frac{\pi}{2} + \lambda - \beta\right)\hat{\imath} + ()\hat{\jmath} + \sin\alpha\hat{k}\right],$$

or

$$0 = -\sin\phi\cos\alpha\sin(\lambda - \beta) + \cos\phi\sin\alpha,$$

or

$$\lambda = \beta + \sin^{-1}\frac{\tan\alpha}{\tan\phi}. \tag{2.1}$$

The difference in time between pulses on S_1 and S_2 is therefore

$$\Delta t = \frac{1}{\omega}\left[\beta + \sin^{-1}\frac{\tan\alpha}{\tan\phi}\right], \tag{2.2}$$

where ω = spin rate. Knowing ω and Δt, we can determine ϕ:

$$\phi = \tan^{-1}\frac{\tan\alpha}{\sin(\omega\Delta t - \beta)}. \tag{2.3}$$

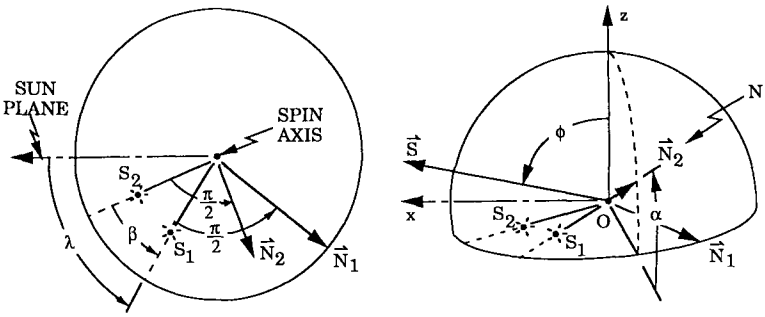

Figure 2.4. Nomenclature for analyzing V-beam slit sensor on a spinning spacecraft.

As an example, suppose that $\alpha = \beta = 35$ deg, $\omega = 16.96$ rad/sec (2.7 rev/sec). Then

Δt 10^{-3} sec	ϕ deg
0	129.3
11.48	120.0
36.01	90.0
73.05	50.0

The accuracy of slit sensors in determining ϕ varies from .001 to 1.0 deg.

ϕ Locates the Spin Axis on a Cone

The angle ϕ determined by the V-beam slit sensor locates the spin axis on a cone that makes an angle ϕ with the direction to the sun (see Fig. 2.5). Another sensor is needed to locate the spin axis on the cone. For example, the first geosynchronous communication satellite, COMSAT II (see Fig. 5.1), had a "pancake antenna beam," which passed over an earth receiving station once every 12 hours (while the spin axis was in the orbit plane, before being precessed to its final position normal to the orbit plane); at the time of peak radiation intensity, the spin axis is perpendicular to the line of sight (LOS) $\vec{OE}$ in Fig. 2.5; hence it lies in the plane OAA' normal to the LOS. Even very coarse dead reckoning resolves the ambiguity between the two possible spin-axis locations OA and OA'.

Problem 2.2.2 – *Satellite with Pancake Antenna Pattern*

Fig. 2.6 shows a satellite in an equatorial geosynchronous orbit whose antenna axis (coincident with its spin axis) is $\vec{TA}$. The beam has a "pancake" shape (see Fig. 5.1).

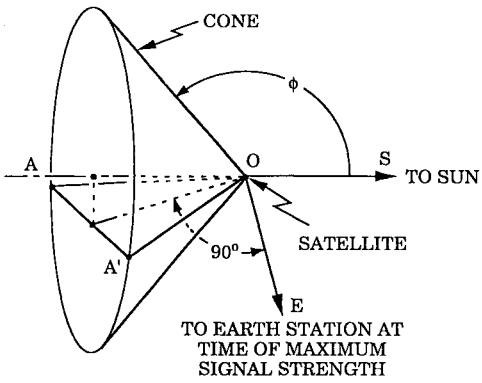

Figure 2.5. Determination of the spin axis orientation from a V-beam slit sensor and a pancake antenna beam.

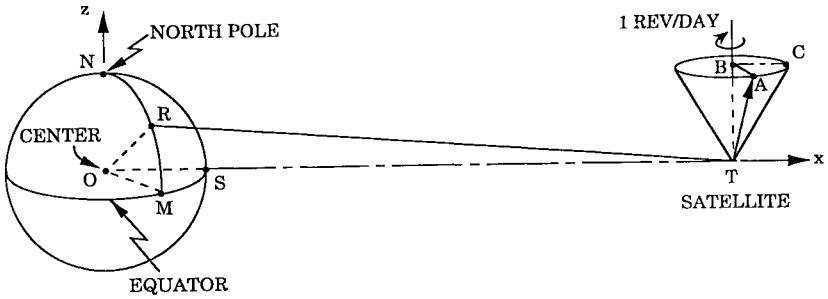

Figure 2.6. Geometrical relations of antenna axis to earth receiving station.

Thus angle $ATR = \alpha$ determines signal strength at an earth receiving station R. Maximum signal strength occurs when $\alpha = 90$ deg.

Let $\vec{TB}$ be parallel to the earth's axis $\vec{ON}$. To an observer at R the satellite spin axis $\vec{TA}$ appears to rotate around $\vec{TB}$ once per day in a clockwise direction (looking from above), because it is fixed in inertial space and the line $\vec{OT}$ rotates counterclockwise once per day with respect to inertial space. Let $\vec{BC}$ be parallel to $\vec{OT}$, and angle $CBA(= \theta_T)$; then $\dot{\theta}_T = 2\pi$ rad/day.

Let ϕ_R = angle ROM = latitude of R, θ_R = angle SOM = difference in longitude of R and S where S is the subsatellite point, ϕ_T = angle BTA, $r_T = \vec{OT}, r_E = \vec{OS}$.

(a) *Show that*

$$\cos\alpha = a\cos\phi_T + \sin\phi_T(b\sin\theta_T - c\cos\theta_T),$$

where

$$a = \frac{r_E}{\ell}\sin\phi_R,$$

$$
\begin{aligned}
b &= \frac{r_E}{\ell} \cos\phi_R \sin\theta_R, \\
c &= \frac{r_T}{\ell} - \frac{r_E}{\ell} \cos\phi_R \cos\theta_R, \\
\ell &= \left|\vec{TR}\right| = \left(r_T^2 + r_E^2 - 2r_E r_T \cos\phi_R \cos\theta_R\right)^{1/2}, \\
\frac{r_T}{r_E} &= 6.628.
\end{aligned}
$$

(b) Suppose the receiving station R is at Los Angeles ($\phi_R = 34$ deg N, longitude = 118 deg W) and the subsatellite point is on the equator at longitude = 40 deg W. *Show that*

$$
\begin{aligned}
\cos\alpha &= .08563 \cos\phi_T + \sin\phi_T(.1241 \sin\theta_T - .9885 \cos\theta_T), \\
&= .08563 \cos\phi_T + .9963 \sin\phi_T \sin(\theta_T - 82.84^\circ).
\end{aligned}
$$

Suppose observations of signal strength at Los Angeles indicate maximum strength ($\alpha = 0$) at midnight and noon and no signal at all from 2 AM to 10 AM and 2 PM to 10 PM. The half-width of the antenna beam is known to be 6 deg. Estimate ϕ_T and θ_T at midnight in Los Angeles.
Answer: $\phi_T = 11.9$ deg, $\theta_T = 58.8$ or 286.9 deg.

2.2.3 *Optical Telescope Sensors*

Attitude Determination Using Two Lines of Sight to Celestial Objects

Optical telescope measurements provide the most accurate determination of attitude (.1 to .0005 deg).

In space, as opposed to in orbit, attitude is usually described relative to the ecliptic plane (the plane of the earth's orbit about the sun), and the vernal equinox (the line from the sun to the earth on March 21). This may be done by giving the Euler angles of a set of body-fixed axes with respect to this "celestial sphere" (see Fig. 2.7), or a set of direction cosines.

If an optical telescope is pointed at a known star, then the declination (elevation angle above the ecliptic plane) and the right ascension (azimuth angle relative to the vernal equinox) of the telescope axis is known from a star table. Let us call this the x' axis (see Fig. 2.7). If the telescope is then rotated in the body to point at another known star (preferably about 90 deg away from the first star), then a z' axis may be defined perpendicular to the plane determined by the two star lines. Finally a y' axis (in the star line plane) is perpendicular to the x' and z' axes.

Attitude may also be determined using the sun line and a star line. This requires that the spacecraft position be known so that the declination and right

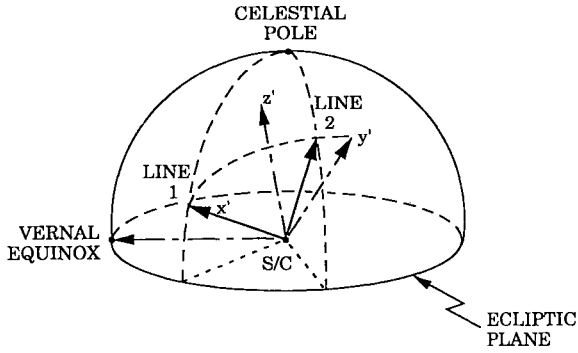

Figure 2.7. Attitude determination using two lines to celestial objects.

ascension of the sun line can be determined. If the spacecraft is in the ecliptic plane, the declination of the sun line is, of course, zero. Many spacecraft use the star Canopus, since it has a high declination and is readily identified.

Planet lines may also be used, but they require a knowledge of the planet position and the spacecraft postion at the time of the sighting so that the declination and right ascension of the planet line can be determined.

Position Determination Using Angles between Celestial Objects

In interplanetary space, position is given in polar spherical coordinates, radial distance from the sun, declination relative to the ecliptic plane, and right ascension from the vernal equinox. Position may be sensed by optical sightings on the sun, the planets, and the stars.

Measurements of the angle between the sun and a planet (or between two planets) locate the spacecraft on a toroidal surface of position, generated by rotating a circle on the planet-sun (or planet-planet) line, as shown in Fig. 2.8. If two other surfaces of position are found, the spacecraft position is determined by the intersection of the three surfaces (there may be more than one possible location).

Measurement of the angle between the sun (or planet) and a star whose direction is known relative to the ecliptic plane and the vernal equinox locates the spacecraft on a conical surface of position generated by rotating the spacecraft-sun (or spacecraft-planet) line about the line of sight (LOS) to the star from the sun (or planet), as shown in Fig. 2.9.

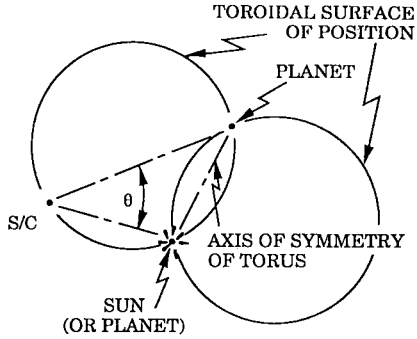

Figure 2.8. Toroidal surface of position for a given angle measurement between the sun and a planet.

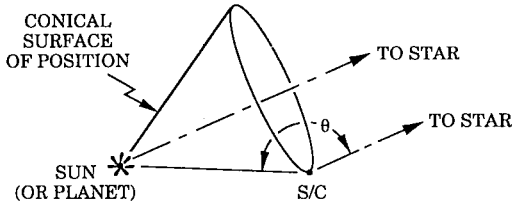

Figure 2.9. Conical surface of position for a given angle measurement between the sun (or planet) and a star.

2.2.4 *Doppler Velocity Sensors*

The velocity of a spacecraft along the line of sight from the earth can be determined very accurately (± 1 cm/sec) by measuring frequency of received electromagnetic radiation from the earth (or vice versa). By the use of Kalman filtering, which involves integrating the measured velocity, radial position can be estimated to an accuracy of a few hundred kilometers a year after the spacecraft has left the earth.

2.3 Orbital Gyrocompassing

Horizon sensors measure roll angle, ϕ, and pitch angle, θ, but they obviously cannot measure yaw angle, ψ. However, if roll-rate and yaw-rate gyros are added (measuring p and r), then it is possible to estimate the yaw angle, using the kinematic roll/yaw coupling described in Equations (1.46) and (1.47):

$$\dot{\phi} = p + n\psi, \tag{2.4}$$

$$\dot{\psi} = r - n\phi. \tag{2.5}$$

If the orbit rate, n, is known, then ψ is observable from (4):

$$\psi = (\dot{\phi} - p)/n. \tag{2.6}$$

Now, the horizon sensor measurement of ϕ is noisy, so we cannot really differentiate the ϕ signal to find $\dot{\phi}$. However, we can construct a kinematic estimator (a steady-state Kalman-Bucy filter), which uses both (4) and (5), along with the measurements of ϕ, p, and r (call them ϕ_m, p_m, r_m), as follows:

$$\dot{\hat{\phi}} = p_m + n\hat{\psi} + K_\phi(\phi_m - \hat{\phi}), \tag{2.7}$$

$$\dot{\hat{\psi}} = r_m - n\hat{\phi} + K_\psi(\phi_m - \hat{\phi}), \tag{2.8}$$

where $(\hat{\phi}, \hat{\psi}))$ are the estimates of (ϕ, ψ). This estimator does not require us to differentiate ϕ_m.

The estimate errors, $\tilde{\phi} = \hat{\phi} - \phi$ and $\tilde{\psi} = \hat{\psi} - \psi$, can be predicted by subtracting (4) and (5) from (7) and (8). If we assume that (ϕ_m, p_m, r_m) are reasonably accurate, then

$$\dot{\tilde{\phi}} = n\tilde{\psi} - K_\phi\tilde{\phi}, \tag{2.9}$$

$$\dot{\tilde{\psi}} = -n\tilde{\phi} - K_\psi\tilde{\phi}. \tag{2.10}$$

The characteristic equation of (9)–(10) is

$$s(s + K_\phi) + n(n + K_\psi) = 0. \tag{2.11}$$

If we wish the error-decay eigenvalues to be $(-n, -n)$, the desired characteristic equation is:

$$(s + n)^2 \equiv s^2 + 2ns + n^2 = 0. \tag{2.12}$$

Comparing coefficients of s in (11) and (12) gives the required gains:

$$K_\phi = 2n, \tag{2.13}$$

$$K_\psi = 0. \tag{2.14}$$

2.4 Gyros

The angular velocity of a spacecraft with respect to inertial space can be determined using three *rate gyros*. If the gyros are attached rigidly to the spacecraft,

then the three measured angular velocities are in body-axis components. If they are mounted on a gimbaled platform, the platform can be servo-stabilized to have nearly zero angular velocity with respect to inertial space. If the platform is initially aligned to be parallel to the ecliptic plane, with one axis pointing toward the vernal equinox, the gimbal angles of this platform are then estimates of the Euler angles of the spacecraft body axes with respect to the celestial sphere. Current inertial platforms drift away from their initial positions at a rate of .01 to .001 deg/hr. Periodic sightings on celestial objects can be used to estimate the platform misalignment; in between sightings the platform provides a good estimate of current spacecraft attitude.

2.5 Inertial Measurement Units

2.5.1 *Inertially Fixed Platform*

For this type of inertial measurement unit (IMU) a platform is mounted in gimbals relative to the spacecraft. Three gyros and three specific force sensors are mounted on the platform with their sensitive axes mutually orthogonal (two in the plane of the platform and one perpendicular to the platform). Using the gyro signals, the gimbals are torqued to keep the angular velocity of the platform as close to zero as possible. The gimbal angles are then the Euler angles of the spacecraft with respect to inertial space (see Fig. 1.3).

The specific force sensors measure the external forces per unit mass on the spacecraft, except for gravitational force per unit mass (since this force acts on both the platform and the proof mass of the sensor). Using the estimated position of the spacecraft, the gravitational force per unit mass can be estimated and added to the signals from the specific force sensors. These signals are then integrated once to give the estimated velocity of the spacecraft with respect to inertial space. These signals in turn are integrated to give estimated position. Note this signal processing involves feedback since the gravitational force per unit mass is determined from the estimated position.

This is a "dead-reckoning" attitude and position system, based on knowledge of initial position and velocity plus measurements of angular velocity and specific force. Since the measurements and the servos are not perfect, the system develops errors that grow with time. The accuracy of inertial-quality sensors is on the order of .01 deg/hr for gyros and 10^{-6} earth g's for specific force sensors. Position or velocity measurements are often used to "update" the IMU, either continuously or at discrete time intervals.

Detailed treatment of IMUs is given in Refs. WR, WE, and KAY.

2.5.2 *Locally Horizontal Platform*

In circular orbit, it is usually more convenient to maintain the platform in a locally horizontal attitude. To do this, the gimbals are torqued to keep roll and yaw rates as close to zero as possible and the the pitch rate equal to the negative of the estimated orbit rate ($-n$). The gimbal angles are then the Euler angles of the spacecraft with respect to the local horizontal and the normal to the orbit plane (see Fig. 1.4).

Alternatively, an horizon sensor is mounted on the platform to measure pitch and roll angles directly, and the gimbals are torqued to keep them as close to zero as possible. The yaw gimbal is torqued to keep the yaw angular velocity as close to zero as possible. A third alternative is to update the first system from time to time with the horizon sensor (instead of continuously).

2.5.3 *Strapdown IMUs*

If the gyros and specific force sensors are mounted rigidly to the spacecraft, instead of on a gimbaled platform, this forms a *strapdown IMU*. A computer is used to estimate the gimbal angles of a "virtual platform" by integrating the rate gyro signals (using the inverse of Equation 1.37). The specific force measurements are resolved into the locally horizontal frame using the estimated Euler angles of the spacecraft.

3

Attitude Control with Thrusters

3.1 Fast versus Slow Attitude Control

If the desired attitude control bandwidth is large compared to orbit rate n, then gravity or magnetic torques are small compared to the required control torques. Hence, they may be treated as disturbance torques, using a free-space model of the spacecraft dynamics. We shall call this *fast attitude control.*

If, on the other hand, the satellite mission is such that a control bandwidth comparable to the orbit rate is acceptable, then gravity or magnetic torques can be used with reaction wheels (or gimbaled momentum wheels; see Chapter 6) to stabilize the satellite *without the use of thrusters.* We shall call this *slow attitude control.* The use of slow attitude control requires careful configuration design to keep disturbance torques acceptably small.

We shall not discuss slow attitude control with passive libration dampers. This type of damping was used in the early days of the space era (Ref. SY) but has been succeeded by improved methods. It is difficult to build lightweight passive dampers that will dissipate energy at the low libration frequencies.

3.2 Fast Attitude Control Using Proportional Thrusters

If the available control torques are large compared to the disturbance torques, and we wish to *stabilize* the spacecraft attitude *with respect to inertial space,* then the attitude motions about the three principal axes are nearly uncoupled, and stabilization about each principal axis may be treated separately (see Fig. 3.1).

A convenient inertial reference system in interplanetary space is the celestial sphere.

In this section, we consider the somewhat unrealistic case where *proportional thrusters* are available to produce torques about each of the three principal axes.

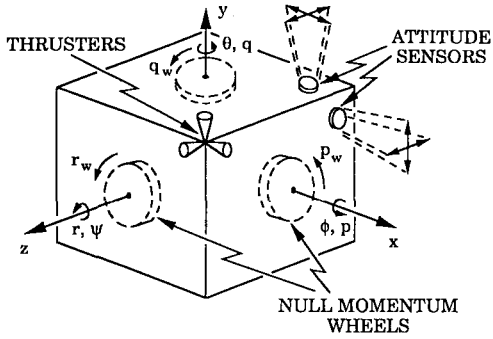

Figure 3.1. Three-axis attitude control thrusters, wheels, and sensors.

Proportional thrusters are *not* easily achieved in practice; we treat them here for pedagogical reasons, since control logic for such thrusters is simpler than control logic for the more practical on-off thrusters, which are treated in the next section.

If *both attitude and attitude rate are sensed* (e.g., using a sun sensor, a star sensor, and three rate gyros), then stabilization about each principal axis may be obtained by feeding back a linear combination of attitude deviation and attitude rate to the torquer. For example, about the body y-axis,

$$Q_y = -D\dot{\theta} - K\theta, \tag{3.1}$$

where

$$I_y\ddot{\theta} = Q_y. \tag{3.2}$$

Clearly, for $D > 0$, $K > 0$, the motion is stabilized.

If *only attitude is sensed* (gyros consume power, reduce reliability, and they cost and weigh more than the devices needed to implement the control logic), then stabilization about each principal axis may be obtained by feeding back attitude deviation with *lead compensation* to the torquer. For example, about the body y-axis,

$$Q_y = -K(\theta - \xi), \tag{3.3}$$

$$\dot{\xi} + b\xi = (b - a)\theta. \tag{3.4}$$

In *transfer function notation*, (2)–(4) become

$$Q_y(s) = -K\frac{s+a}{s+b}\,\theta(s), \tag{3.5}$$

$$\theta(s) = \frac{1}{I_y s^2}Q_y(s). \tag{3.6}$$

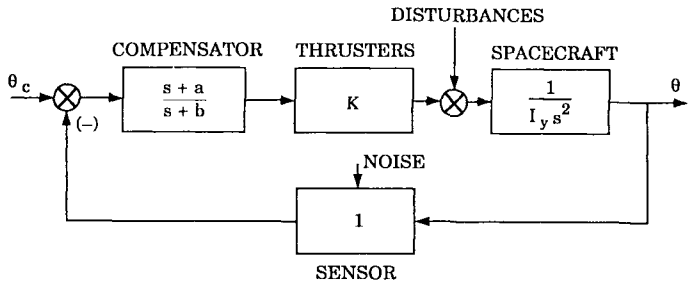

Figure 3.2. Attitude control system with proportional thrusters and attitude sensor.

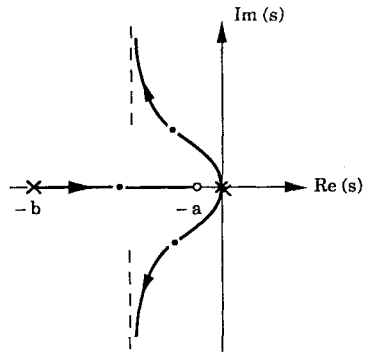

Figure 3.3. Locus of closed-loop roots vs. feedback gain K for system of Fig. 3.2.

Fig. 3.2 shows a block diagram of the system, including the possibility of commanding a nonzero value of θ, called θ_c.

The characteristic equation of the system (5) and (6), in Evans's form, is

$$-\frac{K}{I_y} = \frac{s^2(s+b)}{s+a}. \tag{3.7}$$

Fig. 3.3 shows a root locus versus K for $b > a > 0$. Clearly the attitude is stabilized.

Problem 3.2.1 – *Second-Order Estimator Using Attitude Angle*

Show that attitude-rate q, and attitude θ, may be estimated using a noisy measurement of attitude z_y by the system

$$\dot{\hat{q}} = \frac{Q_y}{I_y} + k_q(z_y - \hat{\theta}),$$
$$\dot{\hat{\theta}} = \hat{q} + k_\theta(z_y - \hat{\theta}),$$

where $k_q > 0, k_\theta > 0$.

Problem 3.2.2 – *Second-Order Compensator Synthesis Using an Estimator*

(a) If we use estimated-state feedback, that is, modify (1) to

$$Q_y = -D\hat{q} - K\hat{\theta},$$

where $\hat{q}$ and $\hat{\theta}$ are obtained with the estimator of Problem 3.2.1, *show that* this yields a second-order compensator, $Q_y(s)/z_y(s)$.

(b) Choose D and K to place the poles of the regulator, (1) and (2) at $s = -\omega_o \pm \omega_o j$, and choose k_q and k_θ in Problem 3.2.1 to place the estimate-error poles at $s = -\omega_o \pm \omega_o j$.

(c) Show that the closed-loop system has double poles at $s = -\omega_o \pm \omega_o j$.

(d) Show that the compensator is

$$\frac{Q_y(s)}{I_y} = -8\omega_o^3 \frac{s + \omega_o/2}{(s + 2\omega_o)^2 + (2\omega_o)^2} z_y(s).$$

(e) Multiply the right-hand side of the equation in (d) by k_o and sketch a root locus versus k_o of the closed-loop system with this compensator. Note for $k_o = 1$, the root locus must have double poles at $s = -\omega_o \pm \omega_o j$.

Problem 3.2.3 – *First-Order Estimator Using Attitude Angle*

Show that attitude rate q can be estimated from a relatively noise-free measurement of attitude z_y, by the system

$$\hat{q} = q^* + \ell z_y,$$
$$\dot{q}^* = -\ell\hat{q} + Q_y/I_y,$$

where $\ell > 0$. Note that

$$\dot{\hat{q}} = Q_y/I_y + \ell(\dot{z}_y - \hat{q}).$$

Problem 3.2.4 – *First-order Compensator Synthesis Using an Estimator*

(a) If we use $Q_y = -D\hat{q} - Kz_y$, where $\hat{q}$ is obtained with the estimator of Problem 3.2.3, show that this yields a classical lead compensator, $Q_y(s)/z_y(s)$.

(b) Choose D and K to place the poles of the regulator (1) and (2) at $s = -\omega_o \pm \omega_o j$, and choose ℓ in Problem 3.2.3 to place the estimate-error pole at $s = -\omega_o$.

(c) Show that the closed-loop system has poles at $s = -\omega_o \pm \omega_o j, -\omega_o$.

(d) Show that the compensator is

$$\frac{Q_y(s)}{I_y} = -4\omega_o^2 \frac{s + \omega_o/2}{s + 3\omega_o} z_y(s).$$

(e) Multiply the right-hand side of the equation in (d) by k_o and sketch a root locus versus k_o of the closed-loop system with the compensation. Note for $k_o = 1$, the root locus must pass through $s = -\omega_o \pm \omega_o j$ and $s = -\omega_o$.

3.3 Fast Attitude Control Using On-Off Thrusters

3.3.1 *On-Off Thrusters*

Proportional gas jets are difficult to build; they usually have a large amount of hysteresis. In addition, proportional valves need open only a small amount to produce the small torques required for control; as a result, dirt and ice particles tend to stick in the valve openings and they do not close completely. The resulting leakage causes the opposing jets to open, and the gas supply dwindles rapidly! Consequently, control techniques have been developed where the valves are either completely open or completely closed ("on-off" or "bang-bang" control). Large springs may be used to hold them shut, thereby reducing leakage; the closing "bang" jars loosen any ice or dirt particles.

Valves can be operated to stay open as little as a few milliseconds and can be fired over a million times reliably, but the valves must stay open a finite length of time, and therefore there is a discrete angular velocity change with each actuation of the valve. As a result, it is not possible to get zero residual angular velocity as it is in principle with a proportional valve.

To prevent opposing jets from fighting each other, there must be a deadband in a system using on-off control. When the vehicle is in the deadband, no control action is taken. When the error signal—which is made up of vehicle attitude and attitude-rate information—exceeds the deadband, then the gas valves are appropriately modulated.

3.3.2 *Bang-Bang Control (No Deadband)*

A simple on-off reaction jet control scheme is obtained using a "linear switching function." If the control torque has only two values (Q_o and $-Q_o$), we can bring θ and $\dot{\theta}$ almost to zero by the control logic

$$Q = -Q_o \, sgn(\theta + \tau \, \dot{\theta}), \tag{3.8}$$

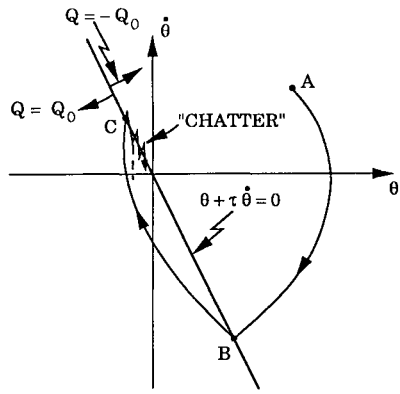

Figure 3.4. Phase plane path of a bang-bang control system with a linear switching function.

where

$$sgn(x) \triangleq \begin{cases} 1 & x > 0 \\ -1 & x < 0 \end{cases}$$

and $\theta + \tau\dot{\theta}$ is the *switching function*, which, in this case, is a linear combination of θ and $\dot{\theta}$. A phase plane diagram of the system behavior is shown in Fig. 3.4.

For Q = constant,

$$\dot{\theta} = \frac{Q}{I}(t - t_o) + \dot{\theta}_o, \tag{3.9}$$

$$\theta = \frac{1}{2}\frac{Q}{I}(t - t_o)^2 + \dot{\theta}_o(t - t_o) + \theta_o. \tag{3.10}$$

Eliminating $t - t_o$,

$$\theta - \theta_o = \frac{I}{2Q}(\dot{\theta} - \dot{\theta}_o)^2 + \frac{I}{Q}\dot{\theta}_o(\dot{\theta} - \dot{\theta}_o) \equiv \frac{I}{2Q}(\dot{\theta}^2 - \dot{\theta}_o^2), \tag{3.11}$$

$$\Rightarrow \dot{\theta}^2 = \frac{2Q}{I}\left(\theta - \theta_o + \frac{I}{2Q}\dot{\theta}_o^2\right), \tag{3.12}$$

which is a parabola in the $\theta, \dot{\theta}$ phase space. The path in the phase space is made up of parabolas until a point like C is reached where the next parabola does not occur to the right of the switching line but starts off to the left; due to the finite time (Δ) necessary to switch the jets off and on, the path actually overshoots the switching line a small amount, and the torque reversal sends the path back

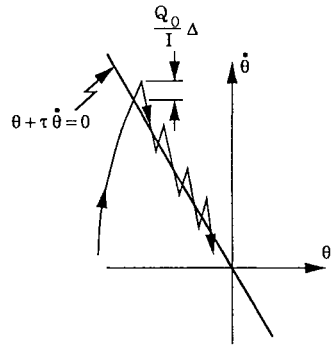

Figure 3.5. Chatter along the switching line in the phase plane.

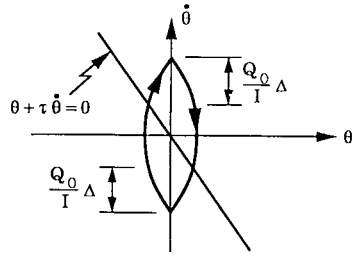

Figure 3.6. Limit cycle around $\theta = \dot{\theta} = 0$, a nonlinear oscillator.

across the switching line, reversal occurs, etc., giving rise to a high-frequency chatter shown in Fig. 3.5.

The path essentially follows $\tau\dot{\theta} + \theta \cong 0 \Rightarrow \theta \cong \theta_c exp(-(t - t_c)/\tau)$, so the system moves toward $\theta = \dot{\theta} = 0$.

The chatter is caused here by the time delay (Δ) in switching the jets on and off. Unfortunately, the point $\theta = \dot{\theta} = 0$ is never reached; instead a *limit cycle* around that point occurs as shown in Fig. 3.6. Obviously this wastes fuel, so some other scheme with a *dead zone* (where $Q = 0$ is used) is desired.

3.3.3 *Bang-Off-Bang Control*

To make effective use of a dead-zone we also use *hysteresis*; dead zone and hysteresis are combined in a scheme called a Schmitt trigger, shown in Fig. 3.7.

It is simple to use the Schmitt trigger with a *linear switching function* as shown in Fig. 3.8.

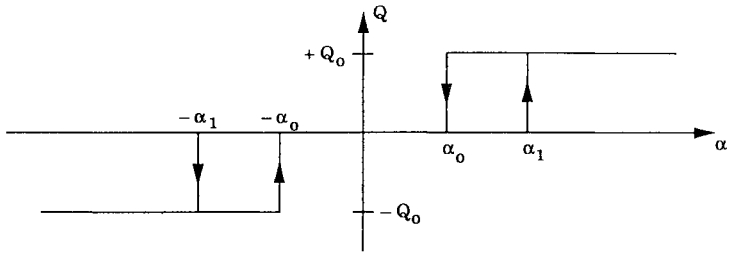

Figure 3.7. Output vs. input with dead zone and hysteresis (Schmitt trigger).

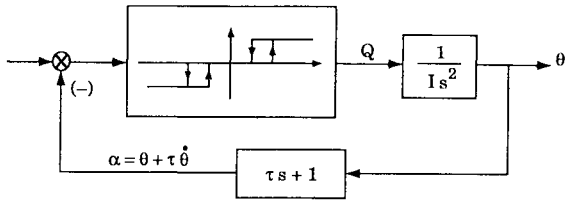

Figure 3.8. Block diagram of Schmitt trigger used with a linear switching function.

This control system cannot bring θ and $\dot{\theta}$ to zero, but at least it can bring them to acceptably small values, ending with a low-frequency limit cycle, which does not use as much fuel as the bang-bang scheme. It is straightforward to show that the limit cycle period and amplitude are given by (see Fig. 3.9):

$$\text{Period} = 4\tau\left(\frac{\alpha_1+\alpha_o}{\alpha_1-\alpha_o}+\frac{\alpha_1-\alpha_o}{2N\tau^2}\right),\quad N\triangleq\frac{Q_o}{I}, \tag{3.13}$$

$$\text{Amplitude} = \frac{1}{2}(\alpha_1+\alpha_o)+\frac{1}{8}\frac{(\alpha_1-\alpha_o)^2}{N\tau^2}. \tag{3.14}$$

Problem 3.3.1 – *Limit Cycle Period and Amplitude*

(a) Given the pitch dynamics

$$I\ddot{\theta} = Q$$

and the Schmitt trigger of Fig. 3.7, verify the expressions for limit cycle period and an amplitude given in equations (13) and (14).

(b) For α_o = 1 degree, α_1 = 3 degrees, $N \equiv Q_o/I$ = 1/3 degree/sec^2 , τ = 5 sec, determine the period and amplitudes of θ and $\dot{\theta}$ in the limit cycle, and plot the limit cycle in the $(\dot{\theta}, \theta)$ plane.

(c) Using the data in (b), calculate the response for $\theta(0) = 30°$, $\dot{\theta}(0) = 0$ and plot the response in the $(\dot{\theta}, \theta)$ plane.

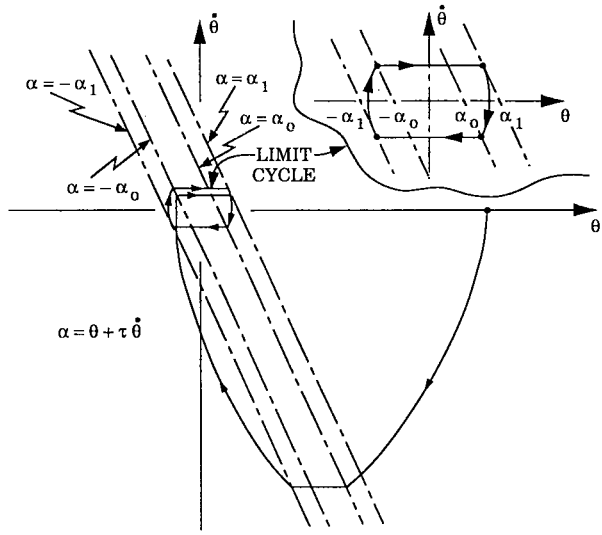

Figure 3.9. Phase plane path; attitude control using deadband and hysteresis (Schmitt trigger).

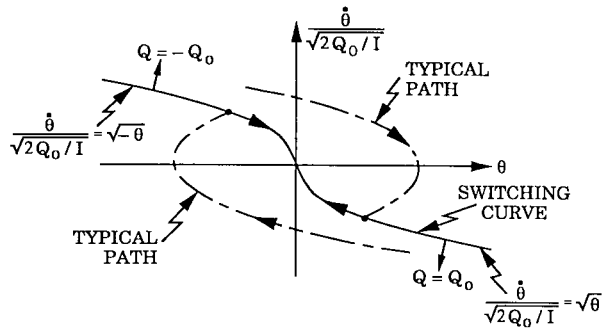

Figure 3.10. Minimum time bang-bang control of attitude (quadratic switching function).

Problem 3.3.2 – *Minimum Time Bang-Bang Control of Attitude*

Minimum-time control of attitude to $\theta = \dot{\theta} = 0$ using two on-off torquers (one for positive torque, one for negative torque) is achieved using the *nonlinear switching* function shown in Fig. 3.10 (see, e.g., Ref. BR-1, pp. 112–13); only one switch is required.

Starting with $\theta(0) = 30°$, $\dot{\theta}(0) = 0$, calculate the time (in units of $1/\sqrt{2Q_o/I}$) to $\theta = \dot{\theta} = 0$ using the linear switching function with $\frac{1}{\tau} = \sqrt{2Q_o/I}$, and with the minimum-time switching function.